The hydrothermal evolution of phase and shape of ZnS nanostructures and their gas-sensing properties

Pengfei Hu[1]*, Guodong Gong [1], Fangyi Zhan[1], Yuan Zhang[2], Rong Li[3] and Yali Cao[4]

[1]Laboratory for Microstructure; [2]Smart Materials Research Center, Materials Genome Institute; [3]Nanoscience & technology research center, Shanghai University, Shanghai 200444, P. R.China

[4]Institute of Applied Chemistry, Xinjiang University, Urumqi, Xinjiang 830046, P. R. China

E-mail: hpf-hqx@shu.edu.cn

This work presents the evolution of the phase and shape of ZnS along the hydrothermal holding time or the dosage of surfactant. **The ZnS sensor obviously showed phase-/defect-dependent gas-sensing performances indicating that the wurtzite-type structure, as well the defect will improve their gas-sensing activities**.

**Keywords:** zinc sulfide, hydrothermal, surfactant, phase evolution, gas sensors

As an important wide band gap II-VI group semiconductor material, ZnS (3.68 eV) has been studied extensively due to excellent electronic and optoelectronic properties.[1-5] ZnS has two phase structures including the zinc blende (ZB, cubic) structure which is a stable phase at low temperature, and the wurtzite (WZ, hexagonal) structure which is a high-temperature stable phase.[6] Some groups carried out a series of work for the phase-controlled synthesis of ZnS nanocrystals. Generally speaking, most of ZnS nanocrystals synthesized via low-temperature solution-phase methods have the ZB structure.[7] And the wurtzite ZnS was mostly prepared by thermolysis of the complex $ZnS(EN)_{0.5}$ (EN = ethylenediamine) precursor in vacuum or solution at high temperature, such as Li et al. and Yu et al. harvested the wurtzite ZnS two-dimensional nanostructures by thermal decomposition of $ZnS(EN)_{0.5}$ precursor at 350-800 ^{o}C or 250/500 ^{o}C in vacuum respectively.[8, 9] Moreover, several low-temperature synthesis strategies have been introduced, such as biological

molecules template approach.[10]

On the other hand, the study for phase transition of ZnS showed that the WZ structure could be transformed spontaneously to the ZB structure at ambient temperature, but reverse transition required rigorous conditions. It has been reported that the bulk ZB ZnS can be transformed to the WZ structure only if the temperature exceeds 1020 °C.[11] Although phase-transition temperature decreased with decreasing particle size, it is often difficult to fall to general ambient range of temperature (below 200 °C), for example, even for ZB ZnS nanocrystal with the size of 2.8 nm, the transition to wurtzite could be achieved in a vacuum at a temperature over 400 °C. [12] It is worth mentioning that hydrothermal treatment is another method for phase transition of nanomaterials, such as titanium dioxide.[13] But the transition from the ZB structure to the wurtzite is difficult under hydrothermal condition, even with hydrothermal treatment of 600 °C for 24 hours.[14] Therefore, how to synthesize ZnS nanostructures with controllable phase composition via low-temperature hydrothermal process still is a challenge.

Recently, the phase-dependent properties have stimulated the enthusiasm of researchers.[15] For example, studies have presented that the luminescent properties of wurtzite ZnS are more excellent than that of ZB ZnS.[16] Huang and Wang reported that the photocatalytic efficiency of zinc blende is higher than that of wurtzite.[17] Another important performance addressed here is their gas-sensitive response for some gas, such as nitrogen dioxide (NO_2),[18] ethanol,[19, 20] hydrogen.[21, 22] However, the study about the relativity about internal microstructure, phase composition of ZnS crystals to their gas-sensing efficiency is still scarce, especially for phase composition.

Herein, we report the hydrothermal synthesis of ZnS with tunable phase composition at 180 °C. The phase composition can be controlled easily by changing the holding time or the dosage of surfactant. Additionally, the influence of the phase composition and microstructure on the gas-sensing efficiency was investigated.
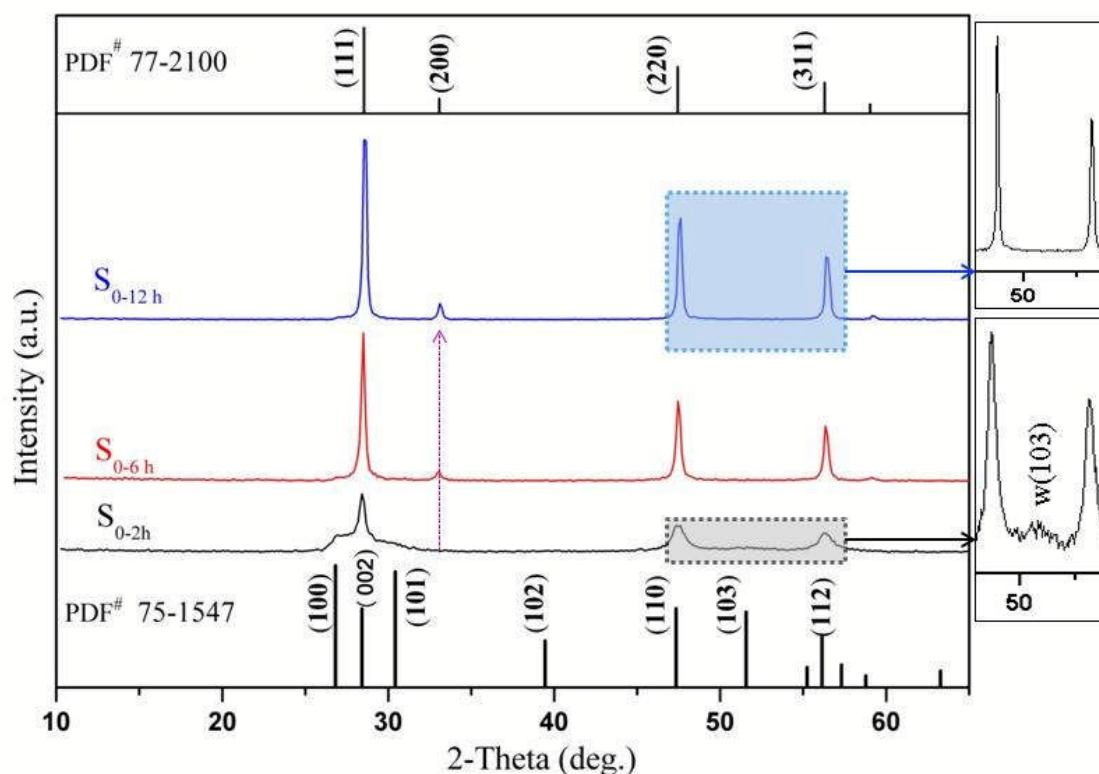
Fig. 1 XRD patterns of the samples obtained with different hydrothermal holding times in the absence of surfactant: $S_{0-2 h}$ 2 hours, S_{0-6h} 6 hours, and S_{0-12h} 12 hours. The upper and bottom of (a) are the standard patterns of standard ZB ZnS (JCPDS card, NO.77-2100) and WZ ZnS (JCPDS card，NO. 75-1547) respectively.
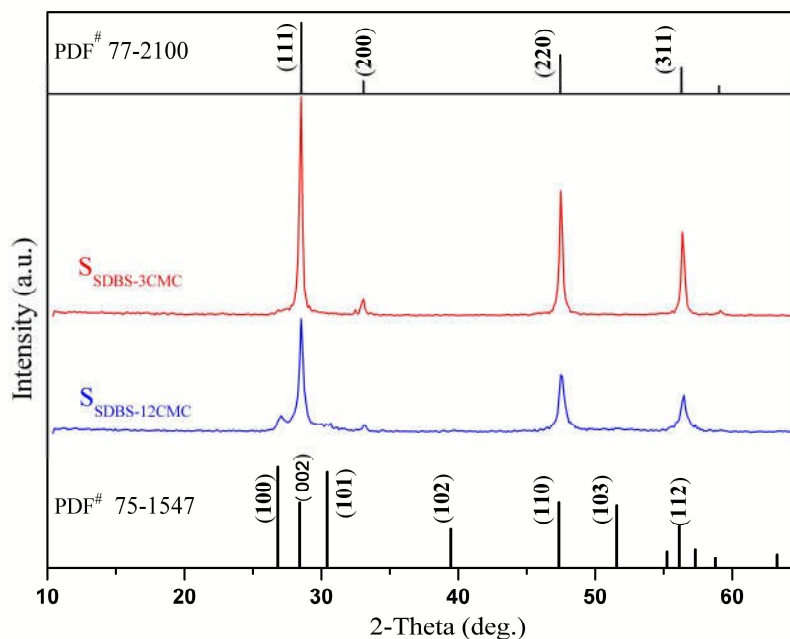
Fig. 1 is the XRD patterns of the samples prepared with different hydrothermal holding times in the absence of surfactant. As shown in pattern S_{0-12h}, all the diffraction peaks are coincident with diffraction peaks of standard ZB ZnS (JCPDS card, NO.77-2100). Interestingly, the S_{0-2h} and S_{0-6h} mainly contain zinc blende, accompanied with the WZ structure which corresponds to the diffraction peaks of the standard wurtzite ZnS (JCPDS card，NO. 75-1547). In comparison, three samples show an increase of the intensity of the s(200) peak and a decrease of w(103) along the holding time, suggesting that the WZ structure gradually transforms to the ZB structure with the prolongation of the reaction time (The study on the evolution of the phase with hydrothermal time were carried out with 20 min, 40 min, and 1 h, but these processes cannot produce ZnS. The exploration on the time node for the pure WZ ZnS is in progress. ESI, Figs S1 and S2 in section S1). The phase composition of

a sample can be calculated from the integrated intensities of the wurtzite (100) peak (2θ) 27.01) and the overlapping zinc blende (111) and wurtzite (002) peaks (2θ) 28.64) as illustrated in literature.[23] The wurtzite phase contents (X_w) of the samples, as well their Brunauer-Emmett-Teller (BET) surface areas and particle sizes (D) estimated from the TEM photographs were listed in Table 1. This demonstrated that the phase composition of products can be adjusted by changing hydrothermal holding time.

Table 1 Phase content, size and Brunauer-Emmett-Teller (BET) surface areas of ZnS nanocrystals

Sample	$X_w{}^a$	D (nm)^b	BET($m^2 \cdot g^{-1}$)
S_{0-2h}	0.184	2.0 μm (made up of 20-50 nm nanoplates)	24.9
S_{0-6h}	0.018	80-150 nm	26.6
S_{0-12h}	0.008	50-150 nm	29.4
$S_{SDBS-3CMC}$	0.017	50-120 nm	30.2
$S_{SDBS-12CMC}$	0.132	20-100 nm (additional about 300 nm plate)	28.5

^{a} Wurtzite proportion of ZnS. ^{b}particle sizes (D) estimated from the TEM photographs (not accept the calculation values from the Scherrer formula $D = 0.89\lambda/\beta\cos\theta$, in which λ is the wavelength of the incident x-rays, β is the full width at half maximum of XRD diffraction peak, θ is the Bragg angle, which is unauthentic).

Fig. 2 XRD patterns of the samples prepared with assistant of surfactant SDBS: $S_{SDBS-3CMC}$ and $S_{SDBS-12CMC}$ represent the samples fabricated with three or twelve times concentration of SDBS respectively.

The XRD patterns of the samples synthesized with the assistant of the anionic surfactant sodium dodecylbenzene sulfonate (SDBS, it is a typical anionic surfactant, some physical properties of it were listed in Table S1 (see ESI, section S2)) were showed in Fig. 2. The analysis of the phase composition according to calculation formula quoted above was also displayed in Table 1. The results show that the X_w will be increased with increasing the dosage of surfactant SDBS. It can be inferred that the surfactant SDBS can hinder the phase transition of ZnS from wurtzite to zinc blende. Additionally, the SDBS is also introduced to control the crystal phase of ZnS in other synthesis methodology, such as microwave-assisted synthesis and solvothermal route.[24, 25] Therefore, the surfactant SDBS can be employed as a new weapon for tuning the phase composition of ZnS.

To sum up, the following trends can be obtained: the WZ phase contents in products will be increased with the shortening of holding time or the increasing of dosage of surfactant SDBS. In addition, the investigations for the effect of other addition agents including PEG-400 (polyethylene glycol 400) and SDS (sodium dodecyl sulfate) were carried out. Experimental results show that they can play the

similar role as SDBS (see ESI, section S3 and Fig. S3).
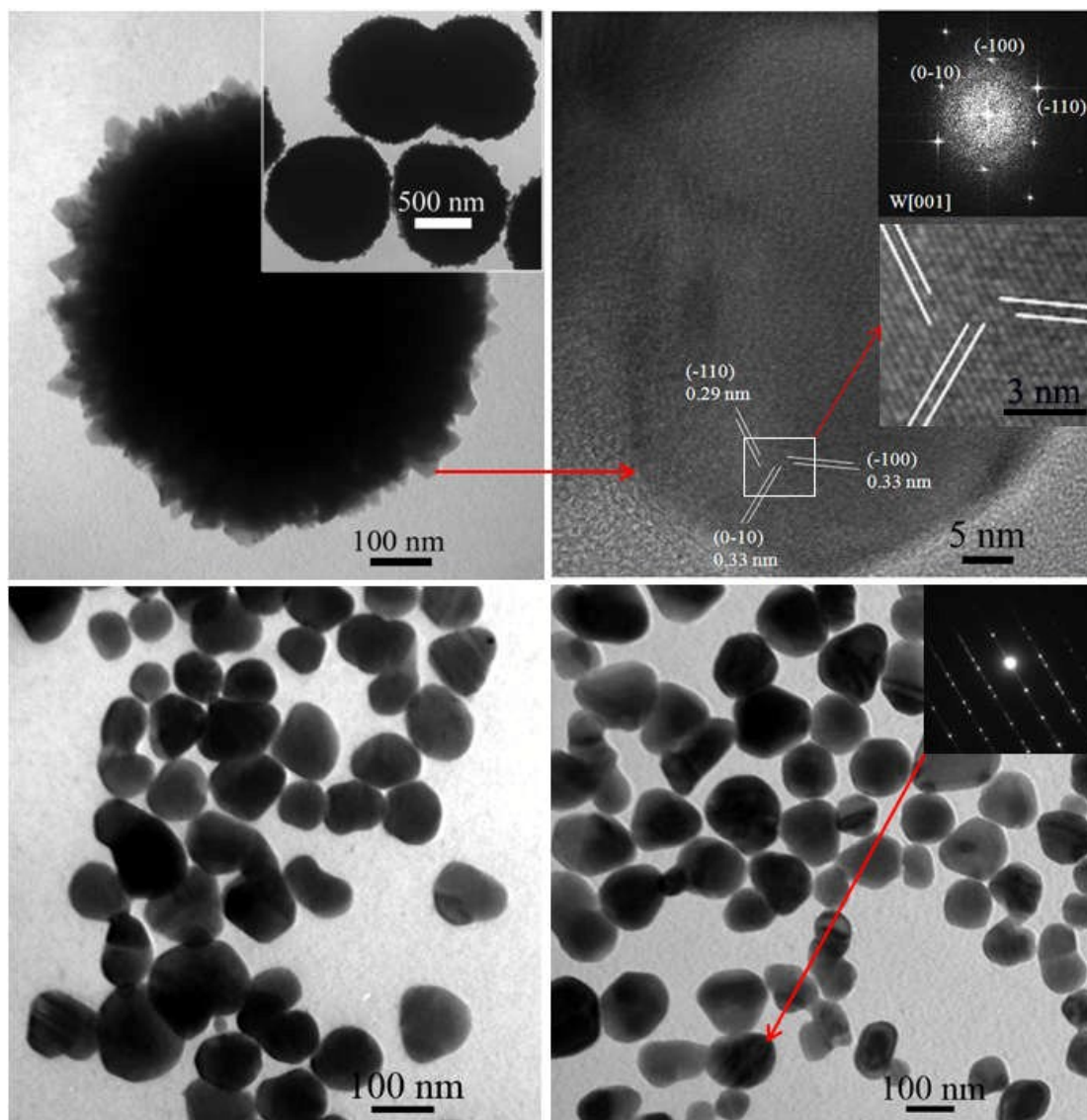
Fig. 3 TEM images of three samples: (a and inset) S_{0-2h}; (b) HRTEM photograph of one nanoflake in a. The upper inset is FFT pattern obtained from this HRTEM image, and the middle inset is a higher-magnification image; (c) S_{0-6h}; and (d and inset) S_{0-12h} and the SAED of a nanoparticle indicated by red arrow.

To investigate the morphological evolution of ZnS nanocrystals along holding time, the samples S_{0-2h}, S_{0-6h}, and S_{0-12h} were examine via TEM and HRTEM, as well select area electron diffraction (SAED) or Fast Fourier Transform (FFT) analysis. As shown in inset of panel a, the products in S_{0-2h} are dominated with spherical objects exposing roughness surface. The average diameter of these spheres is about 2.0 μm. A higher

magnification image of one sphere showed that the roughness of surface comes from some coated flake-like nanocrystals. The microstructures and crystallinities of flake nanocrystals were studied by HRTEM and FFT (panel b of Fig. 3 and inset). The lattice distances of 0.33 nm and 0.29 nm respectively correspond to the distance of the (-100)/(0-10) and (-110) planes of WZ ZnS, and the diffraction spots belong to crystallographic zone axis on the [001] pattern. Unfortunately, the radius of sphere is too large to analyze its internal structure by HRTEM. Combining with above-mentioned analytical results of XRD, here, it is proposed that the product prepared without surfactant may be a core/shell structure. The ZnS sphere may be consisted of a zinc blende core and some wurtzite nanoflakes forming a shell. This is similar to the report by Huang and Banfield,[23] in which they demonstrated that wurtzite grows on the surface of zinc blende particles as a cap. When hydrothermal holding time was prolonged to 6 hours, up to 12 hours, the spherical particles evolved into polyhedral nanoobjects. TEM images in panels c and d show that the shapes of S_{0-6h} and S_{0-12h} are similar. But the size distribution of S_{0-12h} is broader than S_{0-6h}, likely due to the deeper process of Ostwald ripening in S_{0-12h} than S_{0-6h}. Additionally, it is found that some nanoparticles formed the twinning structure (inset in Fig. 3d).
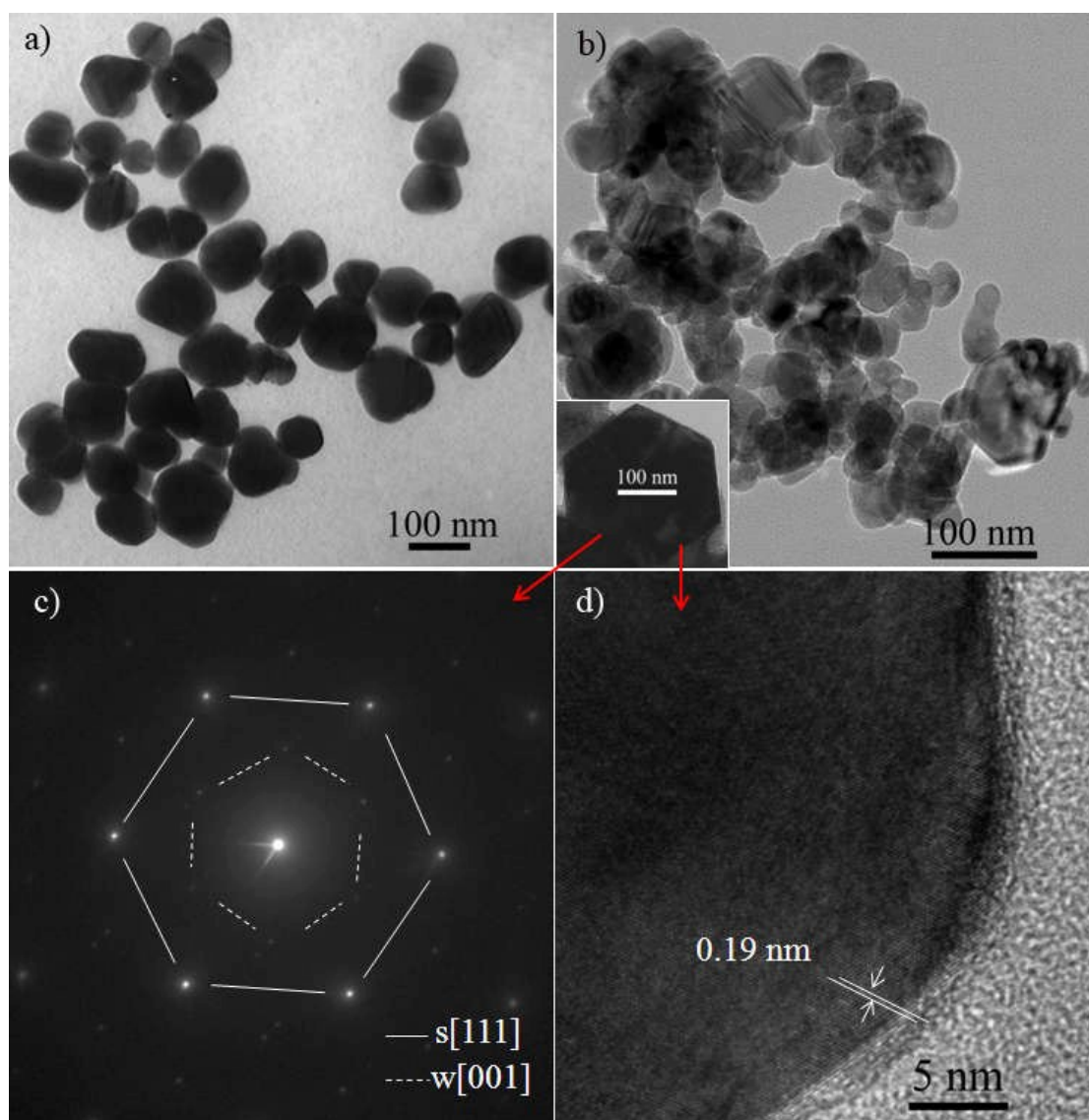
Fig. 4 (a) TEM images of the sample $S_{SDBS-3CMC}$; (b, c, and d) Microstructural characterizations and resolutions of the sample $S_{SDBS-12CMC}$, including low TEM photographs of nanoparticles displayed in b panel, a representative nanoplate shown in inset in b panel, and the SAED and HRTEM resolutions of this nanoplate presented in c and d panels.

Under the presence of SDBS, the shape of ZnS nanoparticles presents more and more changes with increasing the dosage of surfactant. Compared to the sample S_{0-12h}, there was no obvious change in the morphology and size of the nanoparticles in $S_{SDBS-3CMC}$ (Fig. 4a and Table 1). As shown in Figs 4b and its inset, unexpectedly, $S_{SDBS-12CMC}$ mainly contained torispherical and polyhedral particles, accompanied with several hexagonal nanoflakes. In addition, it is worth noting that the size

distribution of ZnS particles is becoming wider and wider along the increase of the dosage of additive. And some small nanoparticles connected each other to form aggregate.

The SAED pattern recorded from the nanoflake in the inset of Fig 4b shows the coexistence of wurtzite and zinc blende structures (Fig. 4c). Hereinto, the ZB structure is main portion which presents its crystallographic [111] zone axis. The nanoflake exposed top and bottom {111} planes, and surrounded by six symmetrical {220} planes. The HRTEM photograph clearly shows the lattice spacing of 0.19 nm corresponding to the distance of {220} planes of ZB ZnS (Fig. 4d). On the other hand, the proportion of wurtzite structure is relatively low which can be confirmed by weak intensity of diffraction spot which presents crystallographic [001] zone axis of wurtzite structure.
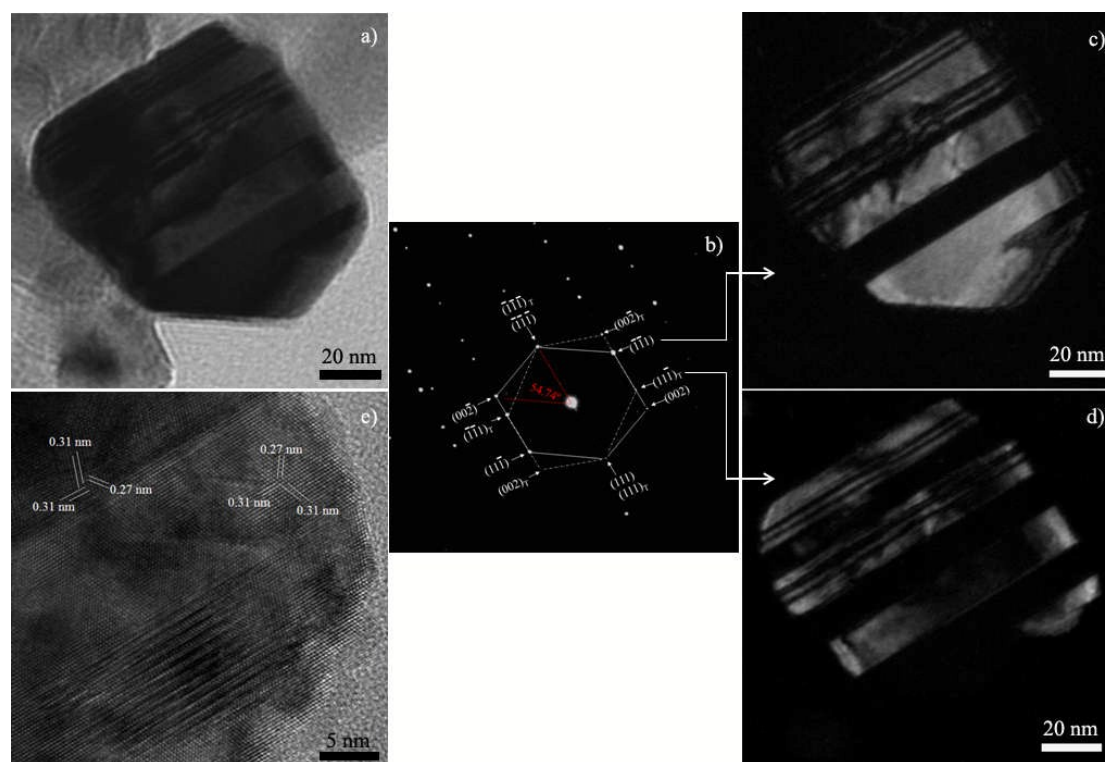
Fig. 5 The structural analyses with electron optics: (a, b, e) TEM image of a representative polyhedral particle in $S_{SDBS-12CMC}$, its SAED pattern, and HRTEM photograph; (c, d) the dark field images of reciprocal twin electron diffraction spot.

Figs. 5a-5e is the TEM photograph of a representative larger polyhedral particle (about 100nm) in $S_{SDBS-12CMC}$ and its structure analyses. Its SAED pattern clearly

showed the characteristics of the {111} twin-substructure and its [0-11] zone axis (Fig. 5b). Figs. 5c and 5d displayed the dark field images of reciprocal twin electron diffraction spot. Moreover, the HRTEM image distinctly indicated these twin structure and the lattice spacing of 0.31 nm and 0.27 nm which correspond to the distance of (111) and (200) planes of cubic ZnS, respectively (Fig. 5e). On the twinning plane and the surface of the nanoparticle would have a great number of defects. Additionally, the HRTEM image of the aggregate (randomly selected) also indicated that the connecting parts between particles have quite a few defects (see ESI, Fig. S4 in section S4). In short, as it were that the $S_{SDBS-12CMC}$ has more defect structures than that in S_{0-6h}, S_{0-12h}, and $S_{SDBS-3CMC}$ (cannot be compared with S_{0-2h} from the TEM resolution).

In order to investigate the cause of the formation of mixed phase, we have changed the source of sulfur and zinc, and carried out the parallel test (see ESI, Fig. S5 in section S5). It was found that the product always is pure zinc blende structure when the sulfur source is replaced by the sodium sulfide, regardless of the length of the hydrothermal reaction time, and whether or not to add the surfactant. On the contrary, another important indication is that the participation of APDC has become a prerequisite for the generation of WZ ZnS.

Based on present experimental results, we have done the following conjectures for the formation of WZ ZnS and the phase transition process. Referring to previous work for the hydrothermal preparation of bismuth sulfide nanocrystals with APDC,[26] here, we also speculated that the APDC firstly chelated to zinc ions to form coordination compound, and then these complexes decomposed to generate wurtzite ZnS nanoparticles under hydrothermal condition. Further research is needed to gain a deeper understanding of the formation of wurtzite ZnS to further verify the above assumption. This work is currently underway in our lab. Secondly, with prolonging the reaction time, the zinc sulfide performs the phase transition from WZ structure to ZB structure, accompanying with morphology and lattice integrity evolution. This process and the functions of APDC and SDBS were speculated and explicated as following.

For ZnS, it is well known that the internal energy of the ZB phase (zinc blende) is slightly lower than that of the WZ phase (the difference between the two phases is quite small, about 13.4 kJ· mol^{-1}).[27] The formation of coordination bonds between the surface zinc atom of ZnS nanocrystallites and organic molecules can lead to a change of the surface energy of ZnS nanocrystallites. When this change overstepped the transition activation energy, it will induce the phase transition from the metastable phase (WZ) to the stable phase (ZB). Yanagida et al. have reported that the WZ structure could be transformed spontaneously to the ZB by contacting with some organic molecules at ambient temperature in 1998.[27] Here, we conjectured that organic fragments derived from $C_5H_{12}N_2S_2$ played a role in this transition, like thiolate or carboxylate anions employed in ref.27. The coordination of these fragments to the surface of ZnS nanocrystallite leads to a change of the surface energy of ZnS nanocrystallites. This change of the surface energy will induce the phase transition from WZ structure to ZB structure at low-temperature hydrothermal process.

In this work, the SDBS plays an important role in the reduction of the size of ZnS nanoparticle and the evolution of their crystal phase. On the one hand, SDBS is a kind of common dispersant, which is widely used to disperse aqueous suspension of inorganic nanoparticles.[28] A dispersion mechanism of SDBS on nanosuspension is proposed as follows: SDBS can give anionic species dodecylbenzene sulfonate by ionization in water firstly. Then, these phenyl sulfonic groups are adsorbed on the surfaces of the nanoparticles and consequently the surfaces are negatively charged. And this leads to the increase of the repulsive forces between the nanoparticles, thereby stabilizing the nanoparticles with small size. Herein, the small nanoparticles increased with increasing the concentration of SDBS supports above discussion (comparing $S_{SDBS-12CMC}$ with $S_{SDBS-3CMC}$). On the other hand, based on the literature, the surface energy of (0001) in WZ structure is lower than that of (111) in ZB structure.[29] At the same time, the molecular dynamics simulation indicates that the surface energy of the (111) surface of the ZB structure will be significantly lowered by adsorbing the SDBS molecule through the sulfonyl group.[24] Therefore, due to the

adsorption of SDBS on the (111) facets of the ZB structure, the transition of the close packing sequence from ccp (cubic close packing, ZB structure) to hcp (hexagonal close packing, WZ structure) could be promoted. That is to say, the X_w of the samples will be increased along with the increase of the concentration of SDBS.

The relationships between working temperature and response of sensor to various gases including ethanol (C_2H_5OH), formaldehyde (HCHO), ammonia (NH_3), methanol (CH_3OH), hydrogen sulfide (H_2S), acetone (CH_3COCH_3), and benzene (C_6H_6) were investigated. The response values to 50 ppm above target gas of the $S_{SDBS-12CMC}$ illustrated in Figs 6a and S6 (see ESI, Section S6). The following conclusions can be obtained from the sensitivity change curves. Firstly, the sensors based on high percent X_w samples S_{0-2h} and $S_{SDBS-12CMC}$ present better gas sensing performance than other samples. Secondly, the gas-sensing response of the sensors shows obvious selectivity, in which, the response to H_2S is particularly prominent in these seven gases. The response value of sensors based on the samples S_{0-2h} and $S_{SDBS-12CMC}$ can reach to 17.5 and 18.0 at the working temperature about 160 ^{o}C for 50 ppm H_2S, respectively, which is higher than other three sensors. At the same time, the results also indicated that the ZnS has lower optimum operating temperature than some other sensing materials such as $ZnFe_2O_4$, and SnO_2/Fe_2O_3 multi-layer thin film. [30, 31]
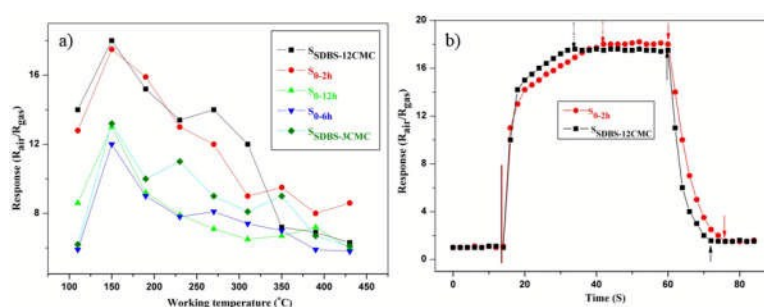
Fig. 6 (a) Relationship between working temperature and response of sensor to H_2S (50 ppm) of various samples. (b) The response and recovery curves for sensors S_{0-2h} and $S_{SDBS-12CMC}$ to H_2S.

That the ZnS brought the high gas-sensing response to H_2S can be illuminated by the fundamental sensing mechanisms of semiconductor, which is described as follows.

It is well known that the mechanism and activity of semiconductor sensor rely on a detectable variation in the resistance when sensor was respectively exposed to the air and the target gas ambient.[32] Semiconductor sensors detect gases primarily by forming a depletion region owing to adsorption of ionized oxygen species on the surface of sensing materials. Firstly, when the sensors are surrounded by air, oxygen molecules are adsorbed on the surface to form chemisorbed oxygen species (O_2^-, O_2^{2-}, and O^-) by capturing electrons from the conduction band of ZnS.[19] Thus, the free electron in the conduction band in the ZnS is decreased, resulting in increased resistance of the sensor, which corresponds to the R_{air}. Secondly, as the ZnS nanoparticles exposed to H_2S gas, the reductive H_2S gas reacts with the oxygen adsorbates, which can be described by following eqn (1) [32, 33]

$$2H_2S + 3O_2^{\alpha-}(ad) \rightarrow 2H_2O + 2SO_2 + 3\alpha e^-, \alpha \text{ is integers 1 or 2}$$

This reaction releases electrons, resulting in a consequent decrease in the resistance of the sensors. The value of resistance is appointed to the R_{gas}.

As to ZnS, it has fertile trapped surface states, sulfur vacancy, and interstitial sulfur lattice defects.[19] These states would facilitate the adsorbing of oxygen molecules from the surroundings. Thus, the free electrons in the conduction band of the ZnS were reduced obviously, resulting in decreased conductivity of the sensor. Herein, the following aspects were suggested to explain the fact that the samples S_{0-2h} and $S_{SDBS-12CMC}$ have better gas-sensing activities than the other three samples, as well their good selectivity to H_2S. Firstly, based on the structure resolution of samples, the two former have lusher defect structure than the latter three. This plays an important role in enhancing their gas-sensing activity by providing more chemisorbed oxygen species for the reaction with the H_2S. Secondly, higher contents of WZ structure of S_{0-2h} and $S_{SDBS-12CMC}$ implied a more mestable WZ structure in them. Thus they are more likely to provide the active sites owing to their high internal energy, leading to the improvment of the gas-sensing performance. The relationship of the wurtzite percent Xw and the response of H_2S is in progress. Furthermore, the wurtzite ZnS nanocrystals mostly present the flake-like shape which exposes the [0001] crystallographic face of wurtzite. A couple of polar planes, Zn-terminated plane and

S-terminated plane of ZnS (i.e., ±[0001] faces), intergenerated on the opposite surface in every nanoflake. The negative S-terminated plane easily brings sulfur vacancy to accommodate oxygen molecules, and then increase the gas-sensing response. Finally, the selectivity of gas sensors to gas may rely on the gas properties, gas–solid reactions,[34] especially the diffusion speed of gas molecules and their different reaction speed with oxygen adsorbates (O_2^-, O_2^{2-}, and O^-) on the surface of sensors. Although the exact reason for the good selectivity to H_2S of ZnS gas sensor remain unclear, but it can be deduced that the diffusion and reaction speeds of H_2S on the surfaces of ZnS nanocrystals are higher than other gases.

In addition, the response/recovery characteristics at operating temperature of 160 °C were investigated. The response/recovery times of sample S_{0-2h} and $S_{SDBS-12CMC}$ to 50 ppm H_2S are 28/16 s and 18/12 s, which is slightly shorter than that for sample S_{0-6h}, S_{0-12h} and $S_{SDBS-3CMC}$ of 19/11 s, 18/9 s, and 20/12 s (Fig. 6b).

In conclusion, a hydrothermal route using organic sulfur source APDC has been successfully employed to prepare the ZnS nanocrystal with tunable phase composition, including wurtzite and zinc blende. The proportion of Wurtzite ZnS in products will be increased with increasing the dosage of surfactant, while it decreased with prolonging the holding time. The hydrothermal assistant of common surfactant SDBS promotes the morphology evolution of ZnS nanoparticles, from polyhedron to quasi-spherical and hexagonal plate-shaped nanoparticles. At the same time, the size distribution of nanoparticles gradually widened. The gas sensors based on ZnS nanocrystals have excellent responsibility and selectivity for H_2S at 160 °C. And the defect and wurtzite structures can improve the gas-sensing activity of ZnS sensor.

Experimental

Preparation

All the reagents are of analytical grade. In a typical procedure for S_{0-12h}, Zinc acetate ($ZnAc_2 \cdot 2H_2O$) and 1-pyrrolidine dithiocarboxylic acid ammonium salt ($C_5H_{12}N_2S_2$, APDC) with a molar ratio of 1:2 were mixed and dissolved in 80 ml distilled water to form a mother solution. After ultrasonic vibration for 10 min, the

above dispersoid was transferred into a 100 ml Teflon-lined autoclave. The autoclave was sealed and maintained at 180 ^{o}C for 12 h, and correlative time-dependent experiments were held 6 h (S_{0-6h}) and 2 h (S_{0-2h}) respectively. Then the autoclaves were cooled down to room temperature naturally. The precipitates were collected and washed with distilled water and absolute ethanol several times, and then dried in vacuum at 60 ^{o}C for 4 h before further characterization.

Other samples ($S_{SDBS-3CMC}$ and $S_{SDBS-12CMC}$) were synthesized following a similar hydrothermal process for the sample S_{0-12h}. Unlike the sample S_{0-12h}, different dosages of surfactant sodium dodecylbenzenesulfonate (SDBS, CMC = 1.2×10^{-3} mol/L, $S_{SDBS-3CMC}$-3.58×10^{-3} mol/L; $S_{SDBS-12CMC}$-1.43×10^{-2} mol/L) were introduced into above mother solution, respectively.

Characterization

The crystalline structures of the products were analyzed by powder X-ray diffraction (XRD, Rigaku D/MAX 2500V/PC X-ray diffractometer) with Cu-Kα radiation ($\lambda = 0.154056$ nm). The morphologies, microstructures, and crystal lattice of the obtained samples were characterized by transmission electron microscopy (TEM, HITACHI H-600, and JEOL JEM-2010F).

Measurements of gas-sensing properties

Gas sensors were made as previously described:[30] The ZnS powders were dispersed in terpineol to form pastes. An alumina ceramic tube, which was assembled with platinum wire electrodes for electrical contacts, was dipped into the paste several times to form the gas-sensing films. Then the elements were annealed at 500 $^{\circ}$C for 1 h to evaporate the terpineol. Finally, the alumina tube obtained with a Ni-Cr heater fixed inside was welded onto a bakelite substrate. To improve the stability and repeatability, the sensors were aged at 300 $^{\circ}$C for 7 days in air prior to use. The test was operated in a glass test chamber using a gas-sensing measuring system of HW-30A (Hanwei Electronics Co. Ltd., PR China), whose device ensures that the target material is in the gaseous state for detection. The working temperature of sensors was adjusted by changing the voltage across the heater side. By monitoring the output voltage across the sensor, the resistances of the sensor in air or in test gas can be

measured. The gas response (response magnitude) of the sensors was determined as the R_{air}/R_{gas} ratio, where R_{air} is the resistance of the thick film sensors in air, and R_{gas} is that in the mixture of testing gases and air. The response time is defined as the time required for the conductance to reach 90% of the equilibrium value after the test gas is injected. The recovery time is the time necessary for the sensor to attain a conductance 10% above the original value in air.

Supporting Information. Some physical properties of SDBS, XRD patterns of ZnS nanocrystals prepared with the assistant of different dosage of PEG-400 or SDS, HRTEM images of the aggregates in $S_{SDBS-12CMC}$, XRD patterns of ZnS nanocrystals prepared with diffrent source of sulfur and zinc, and Relationship between working temperature and response of sensor to C_2H_5OH, HCHO, NH_3, CH_3OH, CH_3COCH_3, and C_6H_6 (respectively, 50 ppm) of various samples.

Acknowledgements

Notes and References

1 K. Boldt, C. Ramanan, A. Chanaewa, M. Werheid and A. Eychmüller, *J. Phys. Chem. Lett.,* 2015, **6,** 2590-2597.

2 K. Virkki, S. Demir, H. Lemmetyinen and N. V. Tkachenko, *J. Phys. Chem. C*, 2015, **119** , 17561-17562.

3 U. K. Gautam, X. S. Fang, Y. Bando, J. H. Zhan and D. Golberg, *ACS Nano*, 2008, **2,** 1015-1021.

4 X. S. Fang, Y. Bando, G. Z. Shen, C. H. Ye, U. K. Gautam, P. M. F. J. Costa, C. Y. Zhi, C. C. Tang and D. Golberg, *Adv. Mater.*, 2007, **19,** 2593-2596.

5 D. Moore and Z. L. Wang, *J. Mater. Chem.*, 2006, **16,** 3898-3905.

6 J. Baars and G. Brandt, *J. Phys. Chem. Solids*, 1973, **34,** 905-909.

7 J. Joo, H. B. Na, T. Yu, J. H. Yu, Y. W. Kim, F. Mu, J. Z. Zhang and T. Hyeon, *J. Am. Chem. Soc.*, 2003, **125,** 11100-11105.

8 Z. X. Deng, C. Wang, X. M. Sun and Y. D. Li, *Inorg. Chem.*, 2002, **41,** 869-873.

9 S. H. Yu and M. Yoshimura, *Adv. Mater.*, 2002, **14,** 296-300.

10 I. A. Banerjee, L. T. Yu and H. Matsui, *J. Am. Chem. Soc.*, 2005, **127,**
   16002-16003.

11 A. R. Verma and P. Krishma, *Polymorphism and polytypism in crystals* Wiley:
   New York, 1966.

12 S. B. Qadri, E. F. Skelton, D. Hsu, A. D. Dinsmore, J. Yang, H. F. Gray and B. R.
   Ratna, *Phys. ReV. B*, 1999, **60,** 9191-9193.

13 K. Sabyrov, N. D. Burrows and R. L. Penn, *Chem. Mater.*, 2013, **25,** 1408-1415.

14 S. Kaneko, H. Aoki, I. Nonaka and F. Imoto, *J. Electrochem. Soc.: Solid-State
   Science and Tecnology*, 1983,**130,** 2487-2489.

15 E. Bellotti, K. F. Brennan, R. Wang and P. P. Puden, *J. Appl. Phys.*, 1998, **83,**
   4765-4772.

16 S. B. Qadri, E. F. Skelton, A. D. Dinsmore, J. Z. Hu, W. J. Kim, C. Nelson and B.
   R. Ratna, *J. Appl. Phys.*, 2001, **89**, 115-119.

17 Y. P. Hong, Z. Lin, J. Huang, Y. J. Wang and F. Huang, *Nanoscale*, 2011, **3,**
   1512-1515.

18 S. Park, S. An, Y. Mun and C. Lee, *Curr. Appl.Phys.*, 2014, **14,** S57-S62.

19 L. Xu, H. W. Song, T. Zhang, H. T. Fan, L. B. Fan, Y. Wang, B. Dong and X. Bai, *J.
   Nanosci. Nanotechno.*, 2011, **11,** 2121-2125.

20 L. H. Zhu, Y. Wang, D. Z. Zhang, C. Li, D. M. Sun,S. P. Wen, Y. Chen and S.
   P. Ruan, *ACS Appl. Mater. Interfaces*, 2015, **7 *(37)***, 20793-20800.

21 M. Hafeez, U. Manzoor and A. S. Bhatti, *J Mater Sci: Mater Electron*, 2011, **22,**
   1772-1777.

22 Z. G. Chen, J. Zou, G. Liu, H. F. Lu, F. Li, G. Q. Lu and H. M. Cheng,
   Nanotechnology, 2008, **19,** 055710.

23 F. Huang and J. F. Banfield, *J. Am. Chem. Soc.*, 2005, **127,** 4523-4529.

24 Y. G. Yu, G. Chen, Y. S. Zhou, Y. Wang and C. Wang, *New J. Chem.,* 2014, **38**,
   486-489.

25 L. Hou and F. M. Gao, *Mater Lett.*, 2011, **65**, 500-503.

26 P. F. Hu and Y. L. Cao, *CrystEngComm*., 2012, **14,** 7694-7700.

27 K. Murakoshi, H. Hosokawa, N. Tanaka, M. Saito, Y. Wada, T. Sakata, H. Mori and S. Yanagida, *Chem. Commun*., 1998, 321-322.

28 X. F. Li, D. S. Zhu and X. J. Wang, *J. Colloid Interface Sci.,* 2007, **310**, 456-463.

29 Z. W. Wang, L. L. Daemen, Y. S. Zhao, C. S. Zha, R. T. Downs, X. D. Wang, Z. L. Wang and R. J. Hemley, *Nat. Mater.*, 2005, **4**, 922-927.

30 Y. L. Cao, D. Z. Jia, P. F. Hu and R. Y. Wang, *Ceramics International*, 2013, **39,** 2989-2994.

31 Z. Jiao, S. Y. Wang, L. F. Bian and J. H. Liu, *Mater. Res. Bull.*, 2000, **35,** 741-745.

32 J. Kim and K. Yong, *J. Phys. Chem. C*, 2011, **115,** 7218-7224.

33 N. Barsan and U. Weimar, *J. Electroceram.*, 2001, **7,** 143-167.

34 Z. T. Liu, T. X. Fan, D. Zhang, X. L. Gong and J. Q. Xu, *Sensor Actuat B-Chem.*, 2009, **136(2)**, 499-509.

Graphical and textual abstract
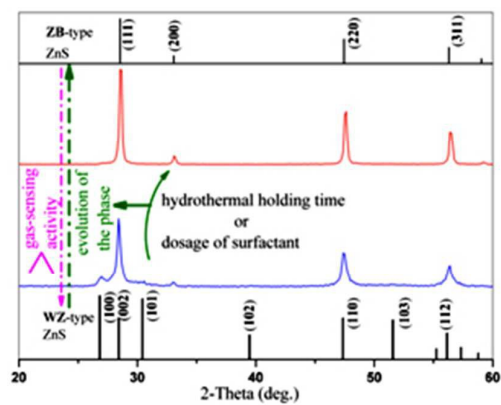
The evolution of the phase of ZnS was achieved by adjusting the hydrothermal holding time or the dosage of surfactant.